



ELSEVIER

1 October 2002

Optics Communications 211 (2002) 31–38

OPTICS  
COMMUNICATIONS

www.elsevier.com/locate/optcom

# Characterization and modelling of the hollow beam produced by a real conical lens

Benoît Dépret, Philippe Verkerk, Daniel Hennequin\*

*Laboratoire de Physique des Lasers, Atomes et Molécules, UMR CNRS, Centre d'Etudes et de Recherches Lasers et Applications, Université des Sciences et Technologies de Lille, F-59655 Villeneuve d'Ascq cedex, France*

Received 1 May 2002; received in revised form 2 August 2002; accepted 7 August 2002

## Abstract

The properties of the hollow beam produced by a conical lens are studied in detail. In particular, the impact of a rounded vertex is examined. It is shown that it could lead to drastic changes in the transverse distribution of the hollow beam, determined by the ratio between the transverse size of the incident beam and the size of the blunt area. An adequate choice for this ratio allows us to either minimize the losses or optimize the distribution symmetry.

© 2002 Elsevier Science B.V. All rights reserved.

PACS: 42.79.Bh; 42.25.-p

Keywords: Diffraction; Axicon; Hollow beam

## 1. Introduction

Axicons are a family of cylindrical symmetrical optical systems that produce a line focus rather than a point focus from incident collimated beam [1]. There are several types of axicons, working either by reflection or by transmission, and being either converging or diverging, but the most common one is probably the conical lens. Such a lens is a cone made with a material of index  $n$ , and a basis perpendicular to its main  $z$ -axis (Fig. 1). An incident collimated beam, propagating along the

$z$ -axis, is deviated towards the main axis of the lens, with an angle  $\beta = (n - 1)\alpha$ , where  $\alpha$  is the base angle of the cone.  $\alpha$  is usually a small angle, typically few degrees or less. Beyond the lens, two zones must be distinguished: in the first one, just after the lens, all deviated beams spatially coexist partially (in the hatched zone of Fig. 1), resulting in a diffraction-free beam. Beyond this zone, beams deviated along different directions do not overlap any more, and the intensity becomes distributed on a ring. Such hollow beams have recently regain interest, in the perspective of their use in optical trapping of atoms [2–4] and Bose–Einstein condensates [5].

These applications require specific properties, as e.g., a zero intensity in the center of the beam, as

\* Corresponding author. Fax: +33-320-337-030.

E-mail address: [daniel.hennequin@unit-lille1.fr](mailto:daniel.hennequin@unit-lille1.fr) (D. Hennequin).

predicted by the diffraction theory [6]. However, in most of the experimental realizations, the obtained pattern is more complicated: a usual observed defect is a drastic asymmetry of the distribution with a tail towards the center, possibly secondary rings and thus a non zero intensity at the center [2]. Practically, this leads to the need of a mask to clean the inner region of the hollow beam, and thus a loss of light power and additional diffraction effects, which are both major inconveniences in the experimental uses of such hollow beams. The source of these differences with respect to the theory is not clearly identified. As the conical lens vertex plays a central role in the transverse distribution of the hollow beam, it is natural to search for the origin of these defects in the properties of this point, in particular by taking into consideration its real shape. In the present paper, we study the modifications induced by the bluntness of the conical lens vertex on the hollow beam transverse shape. We show in particular that the ratio between the transverse size of the incident beam and the size of the blunt area determines the transverse distribution, and that an adequate choice for this ratio allows us to either minimize the losses or optimize the distribution symmetry.

## 2. Geometrical propagation

Fig. 1 describes schematically the geometrical beam propagation through a conical lens. The diffraction-free zone appears between the conical lens vertex V, and the point X where all deviated beams separate. The spatial distribution of the light field in this zone is the superimposition of the interferences between deviated beams and diffraction on the conical lens vertex V. The transverse distribution of the resulting field follows a Bessel function [7]. Its exact nature depends on the shape of the incident beam. For example, an appropriate incident Laguerre–Gaussian beam is able to generate a high-order Bessel beam of arbitrary order [8]. The main interest of Bessel beams is that they propagate without diffraction, i.e., their intensity transverse profile remains invariant upon propagation on macroscopic distances [9]. Bessel beams produced by axicons have been extensively stud-

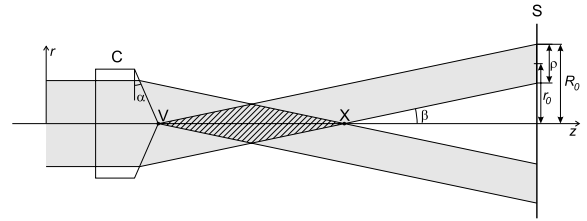


Fig. 1. Schematic behavior, in the geometrical approximation, of a collimated beam through a conical lens C of base angle  $\alpha$ . The propagation axis is the  $z$ -axis, with its origin at the axicon vertex. After the conical lens, the beam is globally deviated towards the  $z$ -axis with an angle  $\beta$ . Point V is on the axicon vertex, while point X corresponds to the abscissa  $z_0$  where a hole appears in the center of the beam in geometrical approximation. The hatched zone between V and X is the Bessel zone. For  $z > z_0$ , the hollow beam has a radius  $r_0$  and a thickness  $\rho$ .

ied, within the framework of numerous applications, such as second-harmonic generation [10], optical parametric generator [11], and atom trapping [12].

Beyond point X, i.e., for  $z > z_0$ , with  $z_0 = r_i/\beta$ , where  $r_i$  is the radius of the incident beam, all deviated beams separate (in the geometrical approximation), and a hole with radius  $R_0 - \rho$  appears in the center of the beam.  $R_0 = \beta z$  is the distance between the  $z$ -axis and the ray crossing the conical lens vertex, while  $\rho$  is the thickness of the ring ( $\rho = r_i$  in the present case). It is also practical to define the radius  $r_0$  of the ring, with  $r_0 = R_0 - \rho/2$  (Fig. 1). Such hollow beams are fundamentally different from hollow Laguerre–Gaussian modes. First, in the last ones, the circulation of the phase around the pattern center is equal to  $2\pi l$ , where  $l > 0$  is the angular index of the mode, while in the axicon hollow beam, it is equal to that of the incident beam, i.e., zero in the case of a plane wave or a  $TEM_{00}$  mode. This phase variation has no consequence on the intensity transverse distribution, but is critical in field dependent systems, e.g., if the hollow beam interferes with another beam. The second point concerns directly the intensity distribution: the axicon hollow beam can be realized with arbitrary ratio between the radius and the thickness of the beam, as both quantities depend differently on  $z$ , while in Laguerre–Gaussian modes, this ratio is fixed by the Laguerre polynomial distribution and does not

vary with  $z$ , except of course if it is transformed by an axicon [13]. Axicon hollow beams can be used in different applications, from laser machining [14] to optical traps for cold atoms [2–4] and Bose–Einstein condensates [5].

### 3. Gaussian beam propagation

In practical realizations, incident beams are often produced by a laser, and thus are gaussian beams. In that case, the incident beam cannot be considered as collimated, but is characterized by a waist  $w_0$  where the beam spot size is minimum. To control the waist location and size, a convergent lens is usually inserted before the conical lens. In particular, it is easy with such a doublet to locate the waist after the conical lens. Fig. 2 shows the propagation of a collimated incident beam through a convergent lens followed by a conical one, in the geometrical approximation. As for collimated beams, an incident ray at the distance  $r$  from the  $z$ -axis, is deviated with an angle  $\beta$ , with  $\beta(r) = (n - 1)\alpha + r/f$ , where  $f$  is the focal length of the convergent lens. We can also define a distance  $z_0$  such that for  $z > z_0$ , a hole appears in the center of the beam. For thin lenses, a simple calculation leads to  $z_0 = r_i(f - d)/(r_i + (n - 1)\alpha f)$  where  $d$  is the distance between the two lenses. As in the single conical lens case,  $R_0$  and  $\rho$ , which now depend both on  $z$ , can be easily calculated. In particular  $R_0 = (n - 1)\alpha z$  has the same value as in the single conical lens scheme. The point focus

in F is transformed in a ring focus of radius  $R_0 = (n - 1)\alpha(f - d)$ , at location  $F' \simeq F$ , where F is the focus point of the convergent lens (the interval between both points is in  $\alpha^2$ ). If the gaussian properties of the incident beam are taken into consideration, all these quantities becomes indefinite, as the transverse expansion of a gaussian beam is theoretically infinite. However, for large incident beams (i.e.,  $w_i \gg \lambda$ ,  $w_i$  being the incident beam size at  $1/e^2$  and  $\lambda$  the wavelength), the geometrical approach remains a good approximation. Therefore, the above expressions, where  $r_i$  is replaced by  $w_i$ , can be used, keeping in mind that they concern  $1/e^2$  intensity limits.

This geometrical approach is unable to describe the thickness  $\rho$  of the ring. To evaluate it, it is necessary to take into account the diffraction of the beam during the propagation, and in particular on the conical lens vertex. Such a theory shows that when the convergent conical lens doublet is illuminated by a gaussian beam, the transverse distribution of the ring at the waist location, is also gaussian, symmetrical with respect to the  $r = R_0$  circle [6]. Its thickness at  $1/e^2$  is  $\rho_0 = 1.65w_0$ , comparable to the beam waist  $w_0$  produced by the converging lens without axicon. The field amplitude of the wave after the lens is given by the usual Fresnel approximation to the Kirchoff integral

$$u(P) = -\frac{i}{2\lambda} \int_S u_i(M)\tau(M)I \frac{e^{ik\zeta}}{\zeta} dS \quad (1)$$

where  $\lambda$  is the wavelength and  $k = 2\pi/\lambda$  is the wave vector.  $u(P)$  is the complex amplitude of the field in point  $P$  of the observation plane,  $u_i(M)$  the incident field in point  $M$  of the diffracting surface and  $\tau(M)$  the transmission function of point  $M$ . The integration is done on the whole diffracting surface  $S$ .  $\zeta$  is the optical distance between  $M$  and  $P$ , and thus  $e^{ik\zeta}/\zeta$  depicts the spherical wave expanding out from point  $M$ . The inclination factor  $I$  depicts the angle of the incident and diffracted beams with the normal to the surface  $S$ . For small apertures and paraxial beams, it is approximated by  $I = -2$ , so that Eq. (1) becomes

$$u(P) = \frac{i}{\lambda} \int_S u_i(M)\tau(M) \frac{e^{ik\zeta}}{\zeta} dS. \quad (2)$$

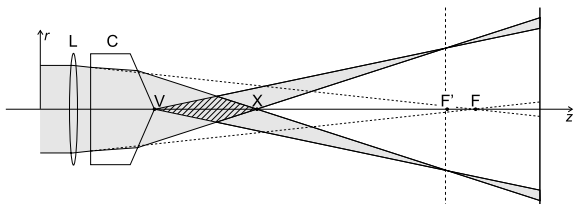


Fig. 2. Schematic behavior, in the geometrical approximation, of a collimated beam through a converging lens L followed by a conical lens C. Point V is on the axicon vertex, while point X corresponds to the abscissa  $z_0$  where a hole appears in the center of the beam. The hatched zone between V and X is the Bessel zone.

The transmission function depends of course on the considered optical elements. It is  $\tau_L(M)$  and  $\tau_C(M)$  for, respectively, a lens and a conical lens

$$\tau_L(M) = \exp\left(-ik\frac{r^2}{2f}\right), \quad (3a)$$

$$\tau_C(M) = \exp(ik(n-1)r \tan \alpha), \quad (3b)$$

where  $r$  is the distance from point  $M$  to the optical axis,  $f$  is the focal length of the lens and  $n$  is the optical index. Eqs. (3a) and (3b) do not take into account a fixed phase shift induced by the thickness of the lenses.

To compute the field amplitude after the conical lens and compare it with experimental measurements, we directly evaluate Eq. (2) through a standard integration software, without any additional approximation. Experimentally, we used a commercial conical lens from Bern optics, with  $\alpha = 2^\circ$  and a radius of 5 mm. It is in BK7 glass with an optical index  $n = 1.51$ . The incident gaussian beam, provided by a laser diode with  $\lambda = 852$  nm, has a waist  $w_i = 645$   $\mu\text{m}$ , so that it can be considered as collimated, and we have  $z_0 = w_i/\beta = 36$  mm. The signal is detected through 2D and 1D CCD cameras, and, therefore, we record the *intensity* of the pattern rather than its field amplitude. Thus the comparison between experimental and numerical results is performed through the intensity transverse distribution.

Let us first illustrate the limits of the present model with a spectacular example: we consider the transverse distribution of the experimental beam described above, at a distance  $z = 115$  mm  $= 3.2z_0$  after the conical lens. Fig. 3 shows the experimental (dashed line) and theoretical (full line) intensity distributions. While the ring diameters are identical, it is clear that the present model is unable to reproduce the details of the distribution. In particular, the experimental profile shows a thin main ring, with inner contrasted secondary rings, looking like diffracting rings. On the contrary, the model predicts a unique thick ring, slightly modulated by diffraction. Thus it is clear that the diffracting elements are not treated correctly in the model.

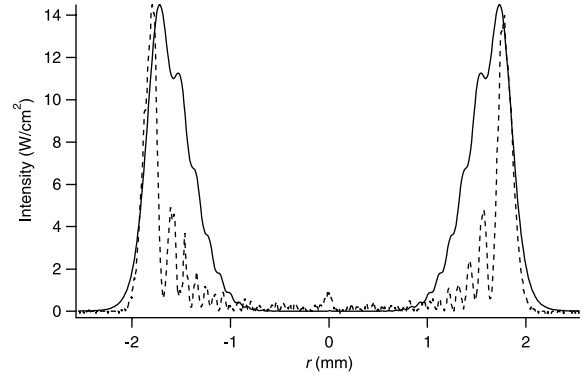


Fig. 3. Experimental (dashed line) and theoretical (full line) transverse intensity profile of the beam in  $z = 115$  mm  $= 3.2z_0$  after the axicon, obtained when the incident beam, with a waist  $w_i = 645$   $\mu\text{m}$ , crosses a unique conical lens. The theoretical profile corresponds to the modelization of the axicon with a punctual vertex. The vertical scale corresponds to the theoretical curve, when the total light power is 100 mW. Units for the experimental curve are arbitrary.

#### 4. Modelling of a real axicon

To enhance the model, we take into consideration the bluntness of the conical lens vertex, by introducing an hyperbolic correction to the conical lens shape (Fig. 4). We introduce the radius of curvature  $R$  of the hyperbole, so that the thickness  $e(r)$  of the lens is

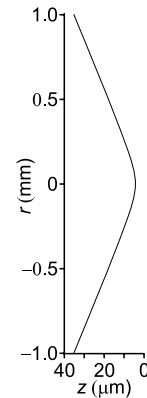


Fig. 4. Schematic representation of the axicon shape taking into account the flatness of its vertex. All parameters are those of Fig. 3, with  $R_{\text{exp}} = 3.5$  mm. The origin of  $z$  is the conical lens vertex.

$$e(r) = e_0 - R \tan^2(\alpha) \sqrt{1 + \frac{r^2}{R^2 \tan^2(\alpha)}}, \quad (4)$$

where  $e_0$  is the thickness of the lens for  $R = 0$ , i.e., when the vertex is a point. To evaluate the radius of curvature  $R_{\text{exp}}$  of our actual conical lens, we use a fit to adjust experimental and theoretical intensity distributions. The best fit, corresponding to  $R_{\text{exp}} = 3.5$  mm, leads to a satisfying concordance between experiments and theory (Fig. 5). The remaining differences between both curves concern the amplitude of the secondary rings, but not their number neither their location. We have also applied our model to non collimated beams, i.e., when the conical lens is used with a convergent lens. As shown on Fig. 6, the transverse distribution of the beam after the doublet is well reproduced. Therefore, the hyperbolic approximation of the vertex appears to be good enough to predict and optimize the use of an axicon to produce a hollow beam.

Fundamental differences appear between the present configuration and the predictions of [6]. In particular, the beam size in the focal plane is almost 2.4 times larger than expected (Fig. 7(a)). If this broadening is effectively linked to the curvature of the conical lens vertex, we expect that it decreases when the incident beam waist increases. Fig. 7(b) shows that indeed, if  $w_i$  is increased significantly, the width of the ring becomes similar to that predicted in [6].

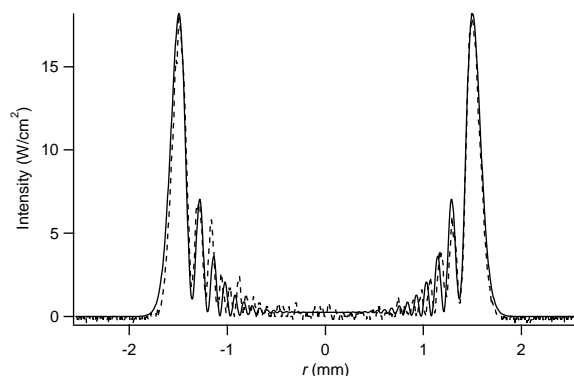


Fig. 5. Same as Fig. 3, except that the theoretical profile corresponds to the modelization of the axicon with the shape of Fig. 4.

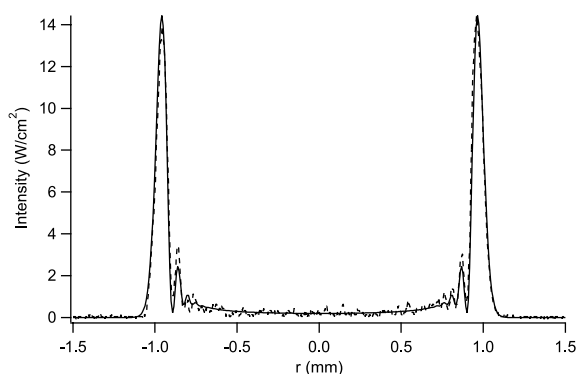


Fig. 6. Experimental (dashed line) and theoretical (full line) transverse intensity profile of the beam in  $z = 65$  mm  $= 2.7z_0$  after the axicon, obtained when the incident beam, with a waist  $w_i = 645$   $\mu\text{m}$ , crosses a convergent conical lens doublet. The convergent lens has a focal length  $f = 100$  mm, and is located at  $z = -10$  mm. The theoretical profile corresponds to the modelization of the axicon with a rounded vertex. Vertical scales as in Fig. 3.

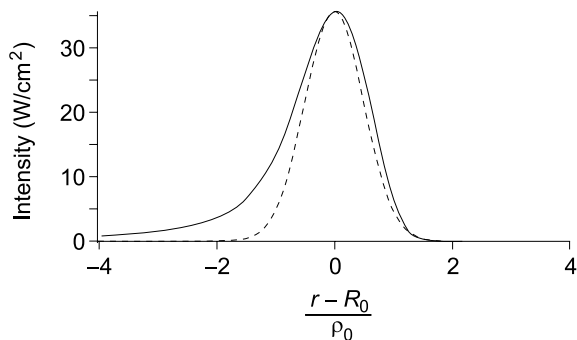
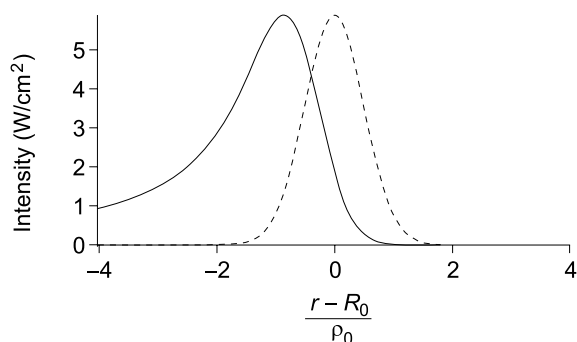


Fig. 7. The full lines show the theoretical transverse intensity profile of the beam in the focal plane of the convergent conical lens doublet for an incident waist  $w_i = 645$   $\mu\text{m}$  in (a) and  $w_i = 3$  mm in (b). The dashed lines gives the gaussian distributions with a width  $\rho_0$ , predicted in [6]. Vertical scales as in Fig. 3.

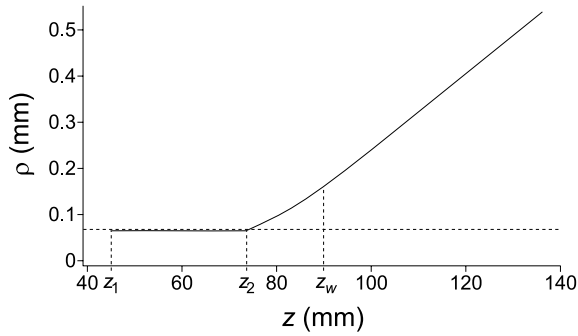


Fig. 8. Intensity distribution thickness versus  $z$ . The width is measured at  $1/e^2$ . The dashed line is the value predicted in the focus plane in [6].  $z_w$  is the abscissa of the focus plane.

Fig. 8 shows how the ring thickness, measured at  $1/e^2$  of its maximum intensity, evolves as a function of  $z$ . Typically, three zones can be defined, delimited by the values  $z_1 \simeq 45 \text{ mm} \simeq 1.9z_0$  and  $z_2 \simeq 75 \text{ mm} \simeq 3.1z_0$ . For  $z < z_1$ , the main peak of the distribution is in  $r = 0$ , as it is typical for the Bessel zone. For  $z_1 < z < z_2$ , the thickness is almost constant, with  $\rho = 1.6w_0 \simeq \rho_0$ , where  $w_0$  is the minimum waist of the single convergent lens, in the focus plane, and  $\rho_0$  is the value predicted in [6]. In the third zone, referred as expanding zone in the following, and corresponding to  $z > z_2$ ,  $\rho$  grows almost linearly with  $z$ . This behavior is very different from that expected. In particular, the narrowest intensity distribution is not in the focus plane, but in the constant zone, just after the Bessel area. However, the smaller ring thickness corresponds to that predicted by [6] in the focus plane, although it occurs outside the focus plane.

But the main novelties of our model concern the shape of the transverse distribution of the intensity. As shown in Fig. 9, very different shapes are obtained in the constant and expanding zone. In the constant zone, the external narrow ring is accompanied by several secondary rings located inside the main one, and separated by dark rings. In the immediate proximity of the Bessel zone, the minimum of the dark rings is almost zero (Fig. 9(a)), and it increases as the expanding zone is approached (Fig. 9(b)). At the edge of the constant and expanding zones (Fig. 9(c)), the contrast between secondary and dark rings vanish, so that in

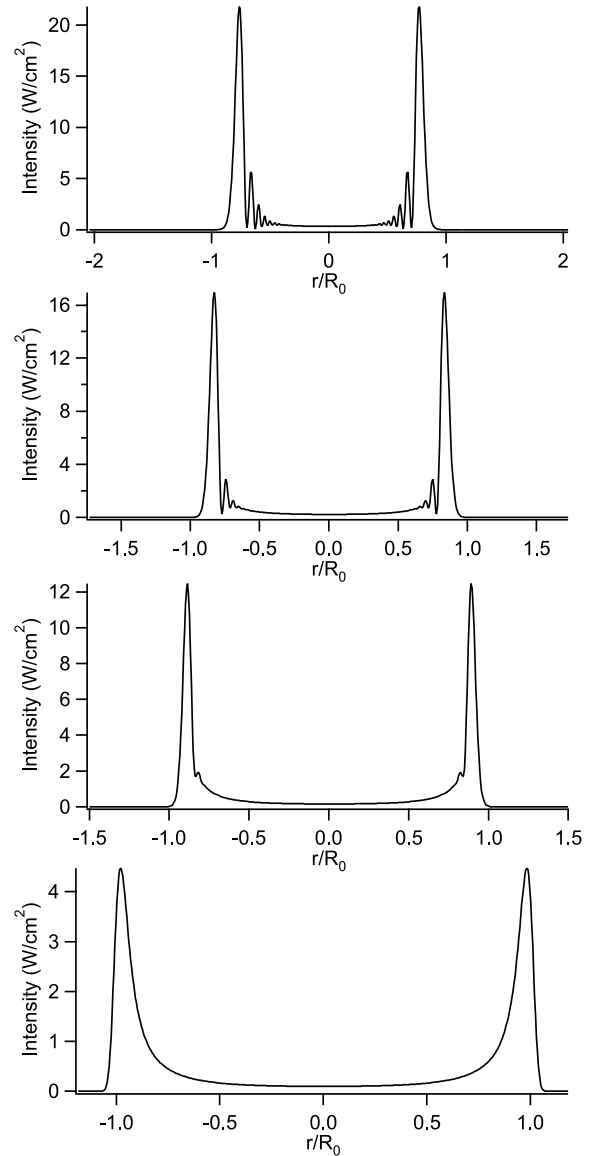


Fig. 9. Theoretical transverse intensity profile of the beam after the convergent conical lens doublet for the same parameters as in Fig. 6 for (a)  $z = 55 \text{ mm} = 2.3z_0$ , (b)  $z = 65 \text{ mm} = 2.7z_0$ , (c)  $z = 75 \text{ mm} = 3.1z_0$  and (d)  $z = 95 \text{ mm} = 4.0z_0$ . All  $r$  axes have the same absolute scale, from  $r = 0 \text{ mm}$  to  $r = 2 \text{ mm}$ . Vertical scales as in Fig. 3.

the expanding zone, the transverse distribution may be described by one single asymmetric ring with a tail towards its center. The resulting pattern in the expanding zone seems to be more clean, but

it requires the use of a mask to suppress the intensity at the center of the ring, leading to new diffracting distortions of the pattern. On the contrary, in the constant zone, and in particular in the proximity of the Bessel zone (in  $z_1$ ), a mask adjusted to the first dark ring cleans the pattern to the single external ring, without additional distortion. The resulting pattern is a single narrow ring with two stiff sides. Thus the constant zone appears to be the most appropriate to produce clean hollow beams.

Another important aspect in the experimental realization of hollow beams is either the total light power inside the final beam, or the peak intensity of the ring. The first point depicts the losses introduced by the mask, while the second one is linked to the thickness of the ring. If the mask is placed at its optimal location  $z_1$ , as described above, it introduces losses of 22%, corresponding to the part of power distributed in the secondary rings. This value has to be compared to that obtained when the mask is placed in the focus plane, as suggested in [6]. In this case, the losses depend naturally on the mask radius, and thus of the ring thickness. To obtain a thickness comparable to that in  $z_1$ , we introduce 40% of losses. To reduce losses to 22%, it is necessary to increase the thickness by a factor 2.3: it is clear that the use of a mask in  $z_1$  produces narrower rings with less losses. As a consequence, as it can be easily realized by comparing Figs. 7(a) and 9(a), the peak intensity of the ring is almost four times larger in  $z_1$  than in  $z_w$ . So from the energetic point of view

also, the technique described above leads to a substantial gain.

In the whole preceding discussion, we have emphasized one given configuration, with a lens with focal length  $f = 100$  mm, with a distance  $d = 10$  mm between the lens and the axicon. The conclusions apply of course to other values of  $f$  and  $d$ . As an example, we illustrate in Fig. 10 the hollow beam obtained for a different set of parameters, using the above technique. The resulting pattern is a single ring with a stiff inner border, and losses introduced by the mask are measured to be  $0.19 \pm 0.01$ , in good agreement with the theory.

## 5. Conclusion

We have shown that taking into account the curvature of the conical lens vertex leads to an accurate description of the beam transformation through a conical lens and a convergent conical lens doublet. Calculations are in excellent agreement with the experiments. We show that the use of a mask allows to obtain an excellent quality hollow beam, assuming that the mask is located adequately, just after the Bessel zone. The quality of the hollow beam consists in a single regular ring, with an intensity going abruptly to zero on its inner side, and no residual intensity in the center of the ring. This enables the use of such beams in interferometric experiments, as e.g., in the realization of optical lattices [15]. In most of the applications, the present system will win in convenience if a second conical lens, located just after the Bessel zone of the first one, is added to the convergent conical lens doublet. Indeed, the second axicon will rectify the phase surfaces and fix the ring radius versus propagation. A third conical lens before the doublet may be added to control independently  $R_0$  and  $\rho$  [16].

## Acknowledgements

The Laboratoire de Physique des Lasers, Atomes et Molécules is “Unité Mixte de Recherche de l’Université de Lille 1 et du CNRS” (UMR 8523). The Centre d’Etudes et de Recherches Lasers

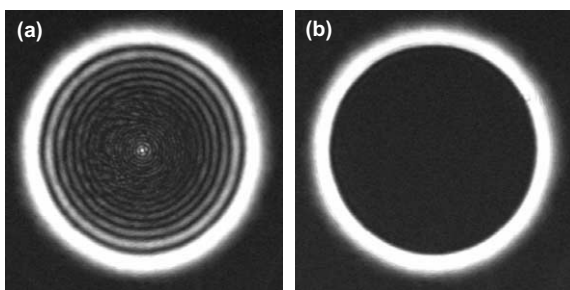


Fig. 10. Experimental record of the intensity pattern obtained in  $z_1$  for the converging conical lens, with  $f = 500$  mm and  $d = 20$  mm. In (a), without the mask; in (b), with a 2 mm mask.

et Applications (CERLA) is supported by the Ministère chargé de la Recherche, the Région Nord-Pas de Calais and the Fonds Européen de Développement Economique des Régions.

## References

- [1] J.H. McLeod, *J. Opt. Soc. Am.* 44 (1954) 592.
- [2] I. Manek, Yu.B. Ovchinnikov, R. Grimm, *Opt. Commun.* 147 (1998) 67.
- [3] L. Cacciapuoti et al., *Eur. Phys. J. D* 14 (2001) 373.
- [4] S. Kulin, S. Aubin, S. Christe, B. Peker, S.L. Rolston, L.A. Orozco, *J. Opt. B: Quantum Semicl. Opt.* 3 (2001) 353.
- [5] E.M. Wright, J. Arlt, K. Dholakia, *Phys. Rev. A* 63 (2000) 013608.
- [6] P.-A. Bélanger, M. Rioux, *Appl. Opt.* 17 (1978) 1080.
- [7] R.M. Herman et, T.A. Wiggins, *J. Opt. Soc. Am. A* 8 (1991) 932.
- [8] J. Arlt et, K. Dholakia, *Opt. Commun.* 177 (2000) 297.
- [9] J. Durnin, J.J. Miceli, J.H. Eberly, *Phys. Rev. Lett.* 58 (1987) 1499;  
J. Durnin, *J. Opt. Soc. Am. A* 4 (1987) 651.
- [10] J. Arlt, K. Dholakia, L. Allen, M.J. Padgett, *Phys. Rev. A* 60 (1999) 2438.
- [11] R. Gadonas, A. Marcinkevičius, A. Piskarkas, V. Smilgevičius, A. Stabinis, *Opt. Commun.* 146 (1998) 253.
- [12] J. Arlt, K. Dholakia, J. Soneson, E.M. Wright, *Phys. Rev. A* 63 (2001) 063602.
- [13] J. Arlt, R. Kuhn, K. Dholakia, *J. Mod. Phys.* 48 (2001) 783.
- [14] M. Rioux, R. Tremblay, P.A. Bélanger, *Appl. Opt.* 17 (1978) 1532.
- [15] B. Dépret, P. Verkerk, D. Hennequin, *J. Phys. IV France* 12 (2002) Pr5-137.
- [16] Y. Song, D. Milam, W.T. Hill III, *Opt. Lett.* 24 (1999) 1805.